Interannual Variability of Summer Water Balance Components in Three Major River Basins of Northern Eurasia

YOSHIKI FUKUTOMI

Frontier Research System for Global Change, Institute for Global Change Research, JAMSTEC Yokohama Institute for Earth Sciences, Yokohama, Japan

HIROMICHI IGARASHI

National Institute for Environmental Studies, Tsukuba, Japan

KOOITI MASUDA

Frontier Research System for Global Change, Institute for Global Change Research, JAMSTEC Yokohama Institute for Earth Sciences, Yokohama, Japan

TETSUZO YASUNARI

Hydrospheric Atmospheric Research Center, Nagoya University, Nagoya, and Frontier Research System for Global Change, Institute for Global Change Research, JAMSTEC Yokohama Institute for Earth Sciences, Yokohama, Japan

(Manuscript received 14 January 2002, in final form 26 September 2002)

ABSTRACT

This study investigated water balance components in the three major river basins of Siberia (the Lena, Yenisey, and Ob) based on the National Centers for Environmental Prediction (NCEP)–Department of Energy (DOE) Atmospheric Model Intercomparison Project II (AMIP-II) reanalysis. The primary focus is the nature of the interannual signatures of summer precipitation, moisture convergence, and runoff in individual basins, and their linkage to the large-scale water transport and circulation fields over northern Eurasia from 1979 to 1995. The temporal characteristics of the hydrological cycle and the associated large-scale circulation structure are discussed.

Some interesting features are found in the interannual variability of basin-scale hydrometeorological elements. In the Lena and Ob basins, the temporal signatures of both precipitation and moisture convergence indicate a cycle of approximately 6 to 8 yr. The mid- and late-summer runoff variation is significantly correlated with these two elements. Moreover, the time series of each element for the Lena is almost exactly out of phase with that for the Ob. The basin-averaged precipitation time series show that the relatively wet phases for the Lena occurred in the early and late 1980s, during relatively dry phases for the Ob. Similarly, the dry phases for the Lena and wet phases for the Ob occurred in the mid-1980s and early 1990s.

The structures of the large-scale moisture transport and circulation anomalies responsible for the precipitation variability for each basin are examined using regression analysis. The space–time fields of precipitation, moisture flux, and geopotential height anomalies are related to the basin-averaged precipitation index. Out-of-phase patterns of precipitation and circulation anomalies between eastern and western Siberia are evident in the regression maps. When the Lena basin is unusually wet, an anomalous cyclonic circulation accompanied by high positive precipitation anomalies is established over the basin, while an anomalous anticyclonic circulation with negative precipitation anomalies is produced over the Ob; the reverse situation is equally evident at other times. Thus, an east–west dipole structure of circulation and precipitation anomalies is formed over northern Eurasia. The ''seesawlike'' interchange of dry and wet regimes associated with this dipole pattern occurs between eastern and western Siberia on a timescale of about 6 to 8 yr. Regression patterns of geopotential height anomalies show good agreement with their summer leading mode derived from a rotated empirical orthogonal function analysis. These results imply that a large-scale mode of atmospheric teleconnective variability modulates the summer hydrological cycle in the northern Eurasian domain.

1. Introduction

Evaluation of the water balance and clarification of hydrological characteristics over the northern Eurasian continental region is one of the important objectives of the Global Energy and Water Cycle Experiment (GEWEX) Asian Monsoon Experiment (GAME)-Siberia project, which was designed to quantify the interactive processes between the atmosphere and land surface, and their relation to patterns of climatic variation. In particular, a study of the nature of the large-scale water balance over northern Eurasia on interannual timescales

Corresponding author address: Dr. Yoshiki Fukutomi, JAMSTEC Yokohama Institute for Earth Sciences, 3173-25 Showamachi Kanazawa-ku, Yokohama City, Kanagawa 236-0001 Japan.
E-mail: fukutomi@jamstec.go.jp

is needed to facilitate understanding of physical linkages with not only regional climatic conditions, but also with various climate subsystems.

During the past two decades, there has been considerable interest in the hydrological cycle in high-latitude land areas. The primary reason is that the water balance in these high-latitude areas is thought to drive the Arctic climate, as reviewed by Walsh (2000). For instance in the Mackenzie River basin, which is a portion of the Arctic drainage area in North America, considerable progress has been made in identifying the connection between the response of runoff to basin-wide precipitation and Arctic climatic variation (e.g., Manak and Mysak 1989; Mysak et al. 1990; Bjornsson et al. 1995). In addition, the atmospheric transport of water vapor into the Arctic basin through this area has been described in several studies (e.g., Walsh et al. 1994; Smirnov and Moore 1999, 2001).

Northern Eurasian hydrology is also considered an important factor controlling the Arctic climate (e.g., Peng and Mysak 1993; Bowling et al. 2000; Serreze et al. 2001a, 2002) and that of the neighboring Asian monsoon area (e.g., Yasunari et al. 1991; Kripalani and Kulkarni 1999). The water from major Eurasian rivers is recognized as an effective source of freshwater flowing into the Arctic Ocean, [see reviews by Bowling et al. (2000) and Carmack (2000)]. Atmospheric moisture transport in high-latitude regions can contribute to the hydrological cycle in the Arctic domain, as discussed in many previous studies (e.g., Cullather et al. 2000; Rogers et al. 2001), because the changes in the characteristics of moisture sources and sinks over the continent may be in response to the moisture input to the Arctic region, and may also play a direct role in the Arctic climate through surface water and energy balances. Several studies have pointed to the significance of the interannual variability of precipitation in the northern Eurasian domain (e.g., Wang and Cho 1997; Ye 2001).

Limited efforts have been made to describe the characteristics of the hydrological cycle and their linkage to large-scale circulation over northern Eurasia, especially in the summer season, when the hydrological cycle is at its most active. Although Ye (2001) identified the various timescales of precipitation variation in this region, he focused only on the winter season. As described below, summer precipitation accounts for about 40% of the annual precipitation over each river basin. In addition, major Eurasian rivers, such as the Lena, Yenisey, and Ob, are recognized as large contributors to freshwater input into the Arctic Ocean (Serreze et al. 2001a, 2002). Summer precipitation and its variability over this continent can be considered an important input to the Arctic freshwater budget.

Peng and Mysak (1993) investigated controls on the long-term variability of the regional summer water balance over the Eurasian basin, and found evidence that summer runoff over western Siberia is strongly affected by precipitation during the preceding winter, which in turn is affected by sea surface temperatures in the North Atlantic and associated teleconnections at interannual timecales. A more recent investigation by Rogers et al. (2001) addressed the importance of water transport into the Arctic region over western Siberia and related atmospheric patterns during summer. In addition, the effort by Serreze et al. (2002) clarified various aspects of the land–atmosphere hydroclimatology in Siberia for all seasons. However, few studies have examined and discussed specific relationships between the basin-scale water balance, including both western and eastern Siberia, and larger-scale circulations for summer. Moisture transport and precipitation during the warm season constitute an integral part of the Eurasian hydrological cycle.

This paper examines the space–time characteristics of the atmospheric hydrological cycle over the northern Eurasian basin during summer (June through August: JJA) employing the National Centers for Environmental Prediction (NCEP)–Department of Energy (DOE) Atmospheric Model Intercomparison Project II (AMIP-II) reanalysis dataset (Kanamitsu et al. 2002). The basin-scale water balance is estimated using a simple budget equation involving precipitation and runoff data. The results are used to discuss the accuracy of water balance estimation using reanalysis products, and to identify climate signals that affect the summer hydrological cycle over Eurasia. We attempt to detect the dominant temporal signals in the water balance components for each of the Lena, Yenisey, and Ob basins, and discuss the coherent atmospheric systems that regulate the basin-scale variation patterns.

The structure of this paper is as follows. Section 2 describes the datasets and the computational procedures used in this study. In section 3, we document the basic features of the annual cycle of water balance components. Seasonal mean and interannual variance of summer precipitation are given. Section 4 presents the dominant temporal signals in the water balance elements for the basins, and the atmospheric sources of those signals, by examining their spatial structure and that of large-scale circulation anomalies occurring simultaneously. Section 5 presents a discussion of the results, and our main conclusions are addressed in section 6.

2. Data and methods

Three observational datasets are used to characterize the water budgets for the individual river basins in this study. One is the NCEP–DOE AMIP-II reanalysis (hereafter referred to as R2) dataset for 1979–99, which has recently been released by NCEP. This data is itemized at 6-h intervals, at T62 horizontal resolution, and 28 sigma levels in the vertical. The horizontal wind and specific humidity from this archive have been used in water budget calculations. Kanamitsu et al. (2002) briefly surveyed this dataset. As they described, the R2 da-

taset resulted from an attempt to improve the quality of the atmospheric and surface components; it is recognized that the former NCEP–National Center for Atmospheric Research (NCAR) reanalysis data (referred to here as R1) contained some errors in atmospheric and surface physical quantities (Kalnay et al. 1996; Kistler et al. 2001). The R2 dataset is believed to estimate the water-related elements more accurately, not only in tropical regions, but also in mid- and high latitudes. Recently, Maurer et al. (2001) derived and compared land surface water budgets for the Mississippi River basin using both the R1 and R2 datasets.

Global precipitation data from surface gauging and satellite-based estimation was presented by Xie and Arkin (1996, 1997); this dataset, called the Climate Prediction Center (CPC) Merged Analysis of Precipitation (CMAP), has also been used to calculate the atmosphere–land water balance and describe the spatial and temporal characteristics of climate signals. This dataset may have advantages for evaluating these components of the continental-scale hydrological cycle. Trenberth (1999) used the CMAP data to estimate precipitation recycling ratio over land on a global scale. Using the combined CMAP and R1 data, a grid-scale atmosphere–land water balance was calculated that suggests that these gauge–satellite merged precipitation data are also applicable to assessments of basin-scale hydrological cycles over an entire continent. The CMAP data has $2.5^\circ \times 2.5^\circ$ resolution on a monthly timescale.

The Bodo-enhanced Russian river flow data were obtained from the NCAR Data Support Section (DSS). This dataset includes data from more than 2400 gauges covering rivers in Russia and the former Soviet Union (FSU) for about 180 yr. We use only the record of discharge and the drainage area information for gauges at the mouths of individual rivers.

In addition to aforementioned datasets, another monthly gridded precipitation dataset for 54 yr from 1948 to 2001 is taken from NCEP–CPC to examine the long-term tendencies of basin-scale precipitation variability. This new product is called PREC/L, which is the precipitation reconstruction over land (Chen et al. 2002). The basic format of this data is almost the same as CMAP data, but is only available over the land area. The NCEP–NCAR monthly reanalysis product is also used for the purpose of additional analysis.

Actual water budget calculations and data analyses were performed for the 17-yr period from January 1979 through December 1995; later runoff data were not available. The available period for runoff data differs for different river basins. The atmospheric water budget equation (e.g., Peixoto and Oort 1992), can be written as

$$\left\langle \frac{\partial W}{\partial t} \right\rangle + \langle \nabla \cdot \mathbf{Q} \rangle = \langle E - P \rangle, \tag{1}$$

where P is precipitation, E is evaporation, and angled brackets denote the area average. Here, the precipitable water content (W), vertically integrated moisture flux vector ($\mathbf{Q}$), and its divergence ($\nabla \cdot \mathbf{Q}$) are defined by

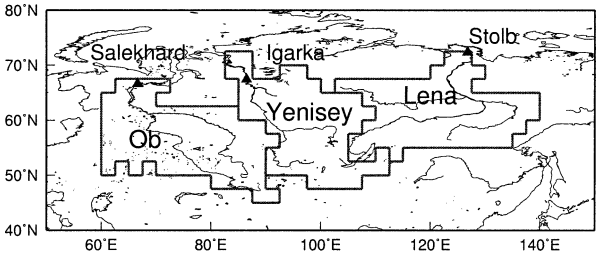

FIG. 1. Three major river basins and the gauge stations measuring the discharge at the river mouths in northern Eurasia.

$$W = \frac{p_s}{g} \int_0^1 q \, d\sigma \tag{2}$$

$$\mathbf{Q} = \frac{p_s}{g} \int_0^1 q\mathbf{v} \, d\sigma \tag{3}$$

$$\langle \nabla \cdot \mathbf{Q} \rangle = -\frac{1}{A} \oint \mathbf{Q} \cdot \mathbf{n} \, dl, \tag{4}$$

where q is the specific humidity, $\mathbf{v}$ is the horizontal wind vector, p_s is surface pressure, g is gravitational acceleration, and σ is the vertical sigma coordinate ($\sigma = p/p_s$; p is pressure). Vertical integration is performed from the top of the atmosphere ($\sigma = 0$) to ground level ($\sigma = 1$). The moisture flux divergence that is the second term in the left-hand side of (1) is computed using the Gauss divergence theorem. The value l represents the boundary of area A, and $\mathbf{n}$ is the unit vector outward normal to A.

The atmospheric water balance was evaluated at both basin and grid scales. The moisture flux divergence at grid scale was computed by applying the spherical harmonic transform method (Adams and Swarztrauber 1999). Evaporation at the land surface was estimated as the residual from the earlier budget equation. Before calculating the moisture flux and other associated elements, a mass correction of horizontal wind fields to eliminate dry airmass imbalances was made, using the method of Trenberth (1991).

The outlines of the three major river basins for which the moisture budget components were computed are shown in Fig. 1. The locations of the gauge sites nearest to the river mouths are also shown. The boundaries of the basins were defined using the gridpoint locations of reanalysis data (2.5° interval), similar to the basin definitions of Oki et al. (1995). Oki et al. (1999) recently produced the Total River Integrated Pathway (TRIP), digitized 1° and 0.5° streamflow basin definitions on a global basis. For this analysis, the perimeters of basins were determined with reference to the TRIP 1° version. The information on the climatological water balance for each basin using these datasets is given in the appendix.

3. Climatological features

a. Annual cycle

Area-averaged water budget estimates were made for three basins, the Lena, Yenisey, and Ob, over a 17-yr period, and the characteristics of the mean annual cycle of their water budget terms are presented before focusing on the summer hydrological cycle. Figure 2 shows the monthly climatological components for each basin; temporal variation is similar to the results presented in the NCEP–NCAR reanalysis (Serreze et al. 2001a, 2002).

The precipitation maximum occurs in July and the minimum in the period from February through March. It is interesting to note that two maxima and two minima of the moisture flux convergence are evident for the Lena and Yenisey. A significant decrease, retaining a low positive value, is evident during the summer. On the other hand, the moisture convergence becomes negative, indicating divergence over the Ob during the summer (June–August); this basin is a moisture-source region during that period. Despite the decrease in moisture convergence, evaporation increases and reaches a maximum in summer over each basin, as does precipitation, emphasizing the importance of surface evaporation relative to the regional water input from precipitation during the summer. Particularly over the Ob, evaporation greatly exceeds the peak value of precipitation during the warm season. These features are similar to the results of Serreze et al. (2002). They discussed different characteristics between basins in the annual cycle of each component, and concluded that larger evaporation and negative $P - E$ for the Ob during summer was due to the specific land cover characteristics and lower atmospheric thermal conditions.

Runoff remains less than 10 mm month^{-1} at each location during the winter and spring; however, it abruptly increases in May and peaks in June, one month earlier than the precipitation maximum in July. This runoff maximum is definitely due to surface discharge of water caused by snowmelt. For the Ob basin, the runoff peak is smaller than those for the other two basins, and the runoff curve indicates smoother temporal changes than in the other two river basins. Serreze et al. (2002) explained this smoother runoff peak by less availability of snow meltwater for runoff, which is caused by the larger evaporation from spring to summer.

The time series of $P - E$ was examined in the same manner (Fig. 2). On a monthly basis, $P - E$ has a value very close to the moisture convergence, but it is adjusted by the W tendency in the budget equation. In addition, the negative values of E derived during the cold season may be caused by underestimating snowfall and rainfall at the rain gauge sites (Serreze et al. 2001a).

b. Climatological fields for summer

The 17-yr climatological fields for the summer (JJA 1979–95), mean precipitation, moisture flux, and its convergence, are shown in Fig. 3a. One of the dominant features is a prominent mid- and high-latitude precipitation band over a broad part of Eurasia. A zonally oriented band of precipitation exceeding 2 mm day^{-1} extending from the east of Lake Baikal to the Far East Asian coast is clearly seen. This band lies along 45°–60°N, which corresponds closely to the area of maximum frontal activity during summer (e.g., Chen et al.

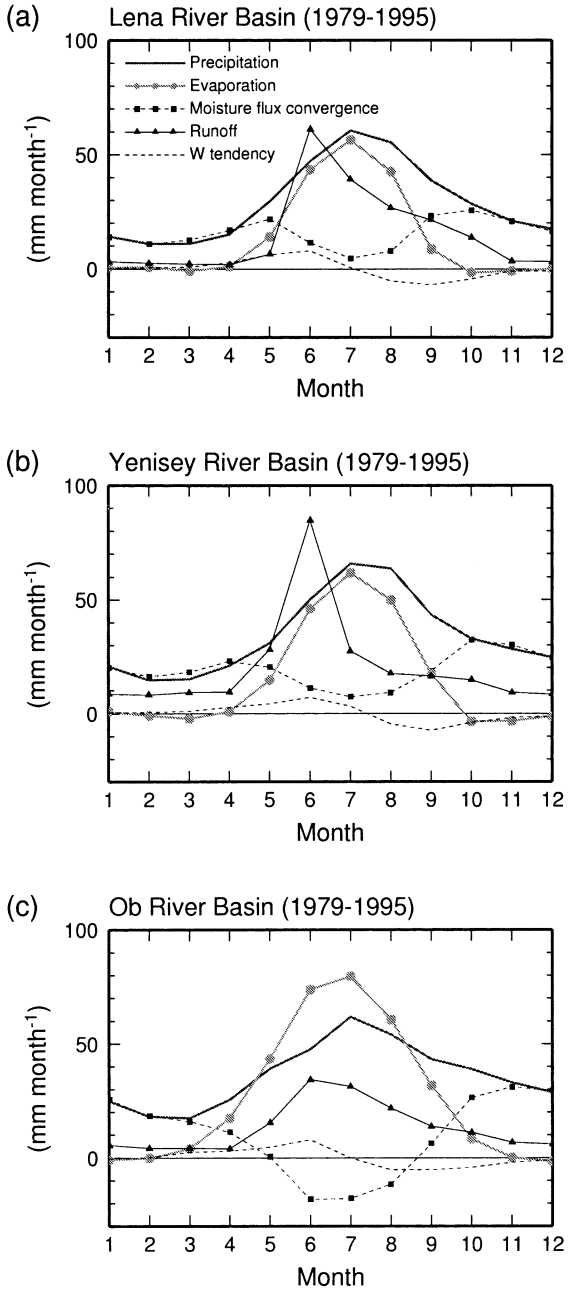

FIG. 2. Annual cycle of precipitation, moisture flux convergence, runoff, and evaporation (estimated as a residual) over the (a) Lena, (b) Yenisey, and (c) Ob River basins (mm month^{-1}). All components except for runoff are 17-yr averages. Runoff records for the Lena and Ob (Yenisey) are available for 16 (17) yr from 1979–94 (1995).

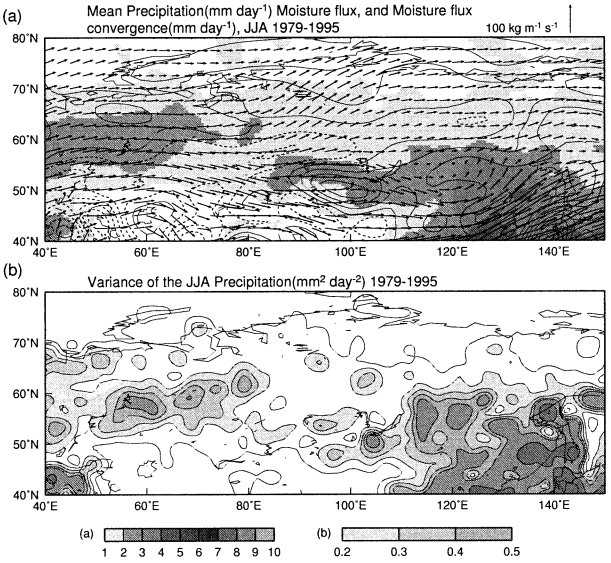

FIG. 3. (a) Average JJA precipitation, moisture flux, and its convergence (1979–95). Precipitation values over 1 mm day^{-1} are shaded. Contour intervals of moisture flux convergence are 0.5 mm day^{-1}. Negative values (for moisture flux divergence) are drawn with dashed contours. (b) Variance in JJA precipitation (1979–95). Contour intervals are 0.1 mm^2 day^{-2} (0.1–0.5) and 1 mm^2 day^{-2} (0.6–2).

1991; Serreze et al. 2001b). This precipitation pattern may be a primary source of water, particularly for the Lena basin during summer. Another band of precipitation extends from northeastern Europe to western Siberia; this constitutes a major water input to the Ob basin. Along these precipitation bands, eastward-directed water transport is prominent, and the moisture convergence maxima almost coincide with the precipitation maxima.

The distribution of interannual variance of JJA precipitation is illustrated in Fig. 3b. Two dominant variance maxima with more than 0.2 mm^{-2} day^{-2} are located over northwestern and eastern Eurasia. One approximately corresponds to the upper Lena basin, and the other covers the Ob basin and the Ural Mountains. The locations of these high-variance centers coincide with those of the mean precipitation maxima shown in Fig. 3a. Also note that the mean and variance of precipitation over the Yenisey basin are both weaker than those over the other two basins. No center of variability for precipitation appears to be dominant over this basin. Substantial interannual variability in the activity of precipitation systems is concentrated in western and eastern Siberia.

4. Interannual variability

a. Interannual signals in hydrometeorological components

This section examines the evidence for a dominant timescale of interannual variability. Figure 4 shows a

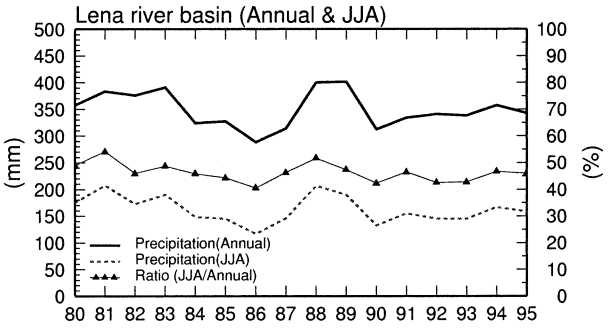

FIG. 4. The time series of annual precipitation (mm), JJA accumulated precipitation (mm), and its ratio to annual precipitation (%) for the Lena River basin.

series of annual precipitation, summer (JJA)-accumulated precipitation, and its ratio to the annual value for the Lena River basin. The annual precipitation is defined as the total amount over the hydrological year from October through September. The ratio for individual years exceeds 40%, emphasizing the importance of summer precipitation. On the other hand, the ratio for the Ob (not shown) is a slightly smaller value, although it still exceeds 30% of the annual precipitation throughout the period of analysis. The percentage for the Yenisey (not shown) is 40%. Another notable feature is the similarity between the long-term changes in JJA precipitation and those of annual precipitation. Temporal-phase characteristics of both time series agree quite well. This suggests that the interannual variation of JJA precipitation contributes significantly to that of the annual precipitation. We note that the JJA precipitation time series appears to have 6–8-yr cycles during our analysis period.

The simultaneous correlation coefficients between the annual and JJA precipitation amounts for individual basins are presented in Table 1. The correlation coefficient for the Lena is 0.95, which considerably exceeds the 95% confidence level (0.45) based on the standard *t* test. This emphasizes the considerable effect of interannual variation in summer precipitation on that of annual precipitation for this basin. For the Yenisey, the correlation coefficient (0.81) is also significant. The value of 0.54 for the Ob is smaller, but still significant.

Figure 5 illustrates interannual variation in the summer hydrometeorological conditions, mean precipita-

TABLE 1. Simultaneous correlation coefficients of summer (JJA) precipitation with annual (Oct–Sep) precipitation in each river basin for 1979–95 (4). The correlation values are above the 95% significance level.

Annual precipitation vs JJA precipitation	
River basin	Correlation coef
Lena	0.95
Yenisey	0.81
Ob	0.54

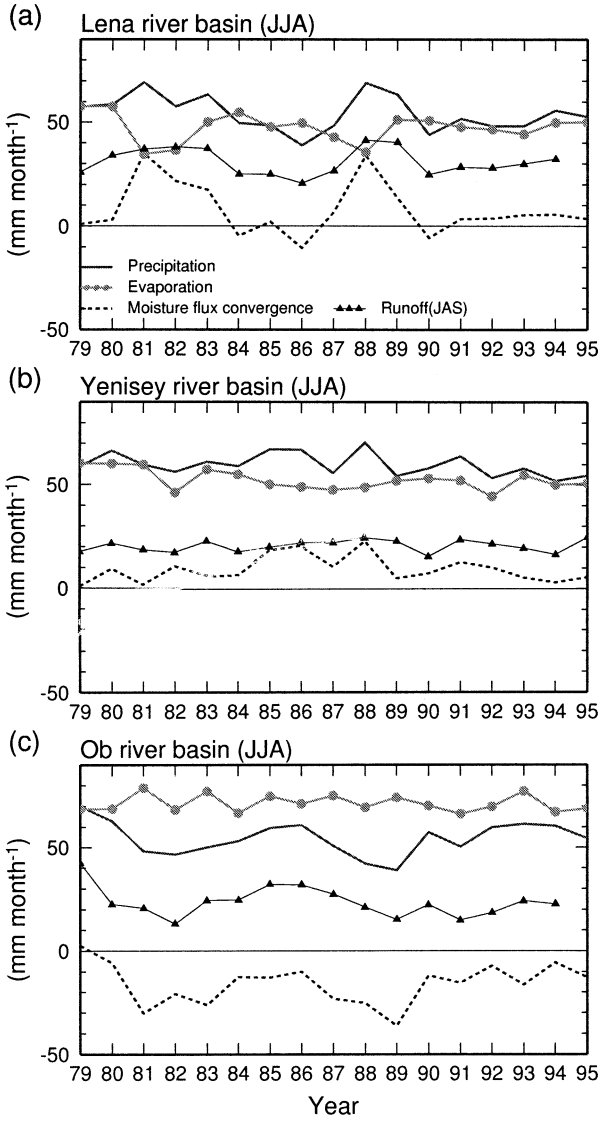

FIG. 5. (a) The time series of JJA averaged precipitation, moisture convergence, evaporation, and JAS averaged runoff for the Lena River basin (mm month^{-1}). (b) As in (a) except for the Yenisey basin. (c) As in (a) except for the Ob basin.

tion, moisture convergence, evaporation as a residual of water balance components, and runoff for each basin. The time series show well-defined interannual timescale signatures. Note that the runoff time series are defined over mid- and late summer from July through September (JAS) in order to reduce the effect of snow meltwater response to runoff.

There is close agreement in the variation among these components, particularly over the Lena (Fig. 5a) and Ob (Fig. 5c). As described above, the time series of the three components has a similar temporal signature. The cross-correlation coefficient between JJA precipitation and JAS runoff is 0.89 for the Lena, and 0.68 for the Ob, as summarized in Table 2. These values are statistically significant at the 95% confidence level.

TABLE 2. Simultaneous correlation coefficients of summer (Jun–Aug) precipitation with summer (Jul–Sep) runoff in each river basin for 1979–95 (4). The correlation values above the 95% significance level are in boldface.

JJA precipitation vs JAS runoff	
JJA precipitation	JAS runoff
Lena	**0.89**
Yenisey	0.32
Ob	**0.68**

Relatively dry and wet periods over each basin are also strongly evident in these time series. In the Lena basin (Fig. 5a), wet years clearly occurred during the early 1980s (1980–83) and late 1980s (1988–89) from the temporal changes of precipitation and moisture convergence. On the other hand, dry periods occurred during the middle 1980s (1984–87) and early 1990s (1990–93). Extreme wet events occurred in the Lena basin in 1981 and 1988, and an extreme dry event in 1986. Interestingly, the precipitation time series for the Ob basin (Fig. 5b) appears to be negatively correlated with that for the Lena basin, with a correlation coefficient of -0.53, which is significant at the 95% confidence level. Relatively dry phases occur in the early and late 1980s in the Ob basin, and wet phases appear in the middle 1980s and early 1990s. Another notable feature in Fig. 5 is the marked difference in the temporal characteristics of the time series for the Yenisey from those of the other two basins. The longer timescale signals seen in the Lena and Ob are not dominant in this basin.

Finally, in this section, we note the temporal variation in residual evaporation derived from observed variables for the basins. Evaporation decreases during the wet phase of precipitation (early and late 1980s) and increases during the dry phase (mid-1980s) in the Lena basin. However, in the Ob and Yenisey basins, such temporal characteristics are not displayed.

b. Large-scale moisture transport and circulation anomalies

This section examines the large-scale moisture transport anomalies and atmospheric circulation patterns associated with the interannual signals in precipitation, as presented earlier. Of particular interest are the spatial structure of moisture transport in the summer precipitation regimes and the coherent pattern of hemispheric circulation anomalies. As shown previously, the centers of action of interannual precipitation variability are located over the Lena and Ob basins. Therefore, we performed correlation and regression analysis between the precipitation in these basins and the large-scale atmospheric fields.

Figure 6a shows the geographical distribution of regressed precipitation and moisture flux anomalies of the June through August seasons when there was a large amount of precipitation over the Lena basin. This anal-

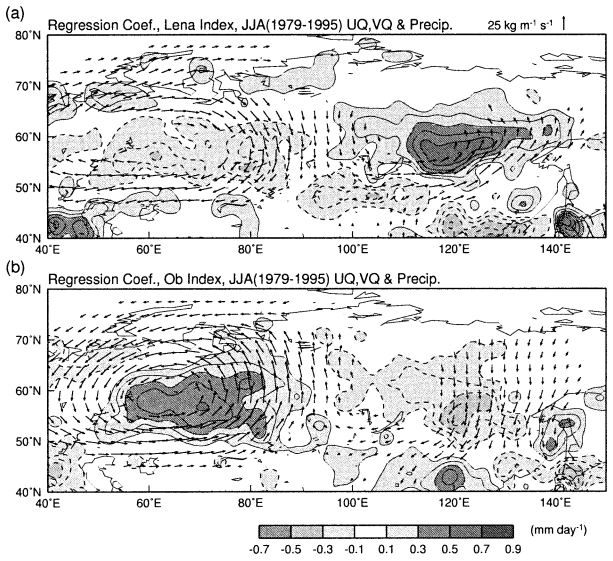

FIG. 6. (a) The regression map of the precipitation (mm day^{-1}) and moisture flux (kg m^{-1} s^{-1}) over northern Eurasia on the precipitation index for the Lena River basin. Contour intervals are 0.1 mm day^{-1}. (b) As in (a) except for the Ob index. Negative values are indicated by dashed contours.

ysis proceeded as follows: A precipitation index was defined as the JJA-averaged precipitation time series (Fig. 5a) with the 17-yr mean subtracted. Linear regression coefficients to estimate precipitation and moisture flux values at each grid point from the precipitation index were then evaluated. A value equal to +1.0 standard deviation of the precipitation index was input to the regression equation to produce the gridpoint values. A test of local statistical significance for the spatial correlation coefficient was performed using the standard *t* test. Only moisture flux vectors with 95% significance were plotted. Positive anomaly patterns on this map correspond to the times when the precipitation index was positive. Therefore, this map represents relatively wet conditions over the Lena basin.

The overall pattern of anomalies in Fig. 6a is characterized by an east–west dipole structure. The positive precipitation anomalies coupled with the cyclonic circulation centered over the upper Lena River basin are well defined. Anomalous eastward and northeastward moisture transport along 45°–55°N appear to contribute to an increased water vapor charge into this basin, and reinforce the precipitation anomalies. On the other hand, negative precipitation and strong anticyclonic moisture flux anomalies entirely cover western Siberia, representing relatively dry conditions in the Ob River basin. It should be noted that the regression pattern of moisture flux convergence (not shown) is similar to that of precipitation. Convergent anomalies prevail over eastern Siberia, while divergent anomalies extend over western Siberia. This suggests that in this situation the Lena basin plays the role of an anomalous moisture sink region, and the Ob a source.

A regression map based on the precipitation index for the Ob (Fig. 6b) was produced, and indicates conditions of increased precipitation in this basin. This map clearly shows a pattern almost completely out of phase with that in Fig. 6a. Compared with Fig. 6a, anomalous wet and dry regions are completely interchanged. Strong positive precipitation anomalies accompanied by cyclonic circulating moisture flux anomalies that are zonally elongated broadly cover western Siberia, and negative precipitation and anticyclonic moisture flux anomalies lie over eastern Siberia.

In order to establish the basic pattern of large-scale circulation anomalies associated with basin-scale precipitation variability, a regression map between the precipitation index for the Lena and 500-hPa geopotential height anomalies over the entire Northern Hemisphere is given in Fig. 7a. This map was constructed in the same manner as Fig. 6a. A clear wave train along 40°–70°N extends from western Eurasia into the North Pacific–Alaska. The spatial scale of these hemispheric wavelike anomalies is at about zonal wavenumber 3 to 4. It is obvious that a significant pair of anomalous cyclone and anticyclone patterns over Eurasia, part of this Eurasian wave pattern, coincides with the east–west dipolelike anomalies shown in Fig. 6a. Additionally, the regression map of geopotential height anomalies based on the Ob index (Fig. 7b) shows a phase signature nearly opposite to the pattern in Fig. 7a, as in the case of Fig. 6b. A series of features found in Figs. 6 and 7 strongly suggest that an east–west ''seesawlike'' replacement of the relative dry and wet regimes occurs on an interannual timescale over the northern Eurasian region.

It is interesting to note that Rogers et al. (2001) also identified the summer wave pattern over northern Eurasia in association with the interannual variation of July poleward moisture transport across 70°N. Comparing our regressed patterns (Fig. 7) with their composite 500-hPa height patterns, one can notice that there are some differences. The most significant difference is the location of Eurasian cyclonic–anticyclonic couplet. While the centers of cyclonic and anticyclonic anomalies in their Fig. 17 are positioned over the Arctic coastal region (70°–80°N), those in our maps lie over the inland area (55°–65°N). The patterns in Fig. 7 rather resemble the composite maps constructed based on *P–E* time series for the Lena River basin by Serreze et al. (2002).

Finally, we present results from a rotated EOF (REOF) analysis using the covariance method performed on the 17-yr 500-hPa geopotential height time series. Its purpose was to establish whether the large-scale anomalies shown by Fig. 7 are directly connected to the atmospheric principal mode for summer on an interannual timescale. Before undertaking the REOF analysis, we carried out an EOF analysis and the first six EOF modes were rotated by the varimax method to obtain the REOF modes. The first REOF (REOF 1; Fig. 8a) pattern is characterized by a zonally extending wave train over mid- and high-latitude Eurasia and the North

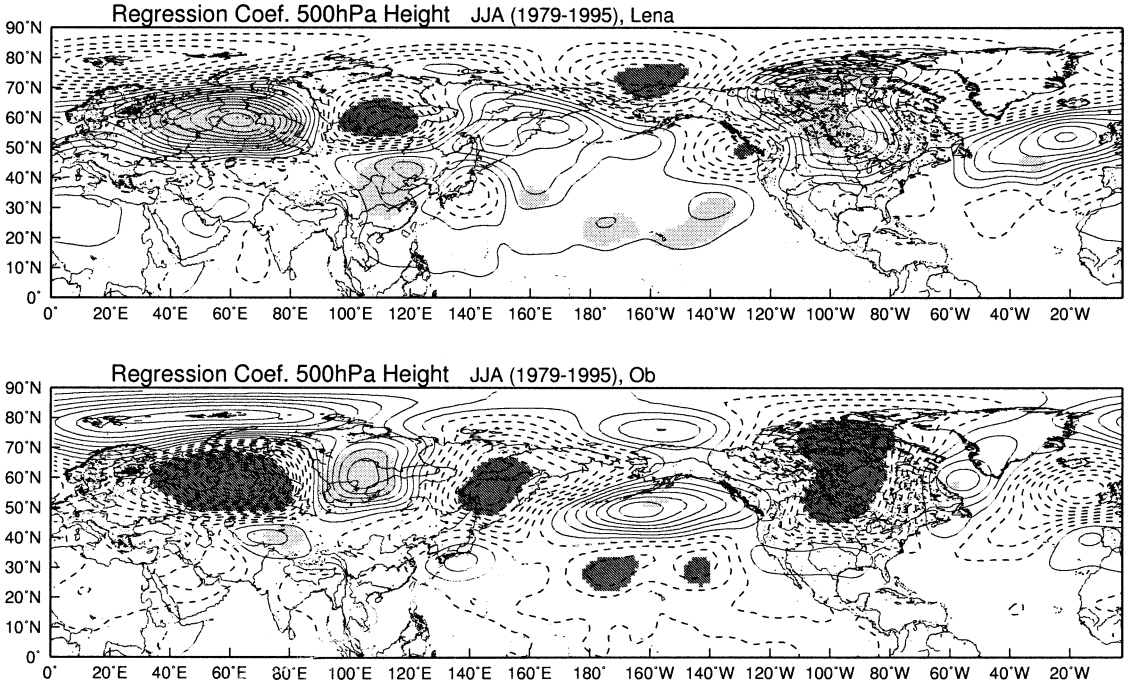

FIG. 7. (a) The regression map of the Northern Hemisphere 500-hPa geopotential height field (m) based on the precipitation index for the Lena River basin. Contour interval is 2 m. Negative values are drawn with dashed contours. Zero contours are omitted. The 95% statistically significant areas are shaded. (b) As in (a) except for the Ob index.

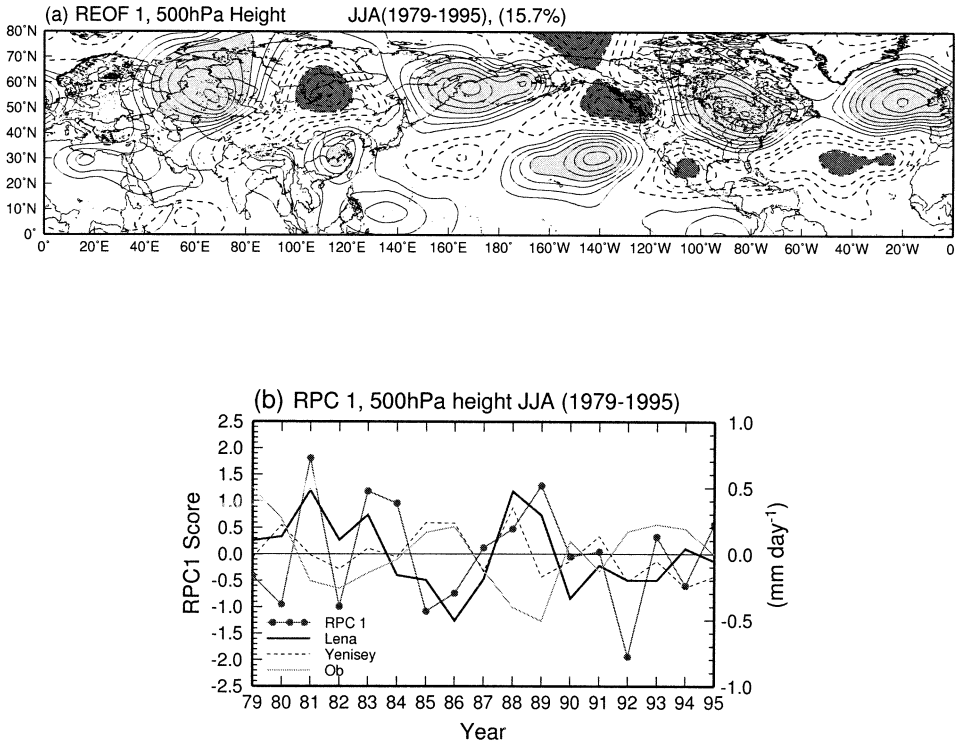

FIG. 8. (a) The REOF1 of the 500-hPa geopotential height field for 17 summers (JJA 1979–95). Contour intervals are 0.1. Negative values are drawn with dashed contours. Zero contours are omitted. Values greater (smaller) than 0.4 are lightly (darkly) shaded. (b) Amplitude time series for the RPC 1 (normalized) and area-averaged precipitation anomalies (precipitation index) for the river basins (mm day^{-1}).

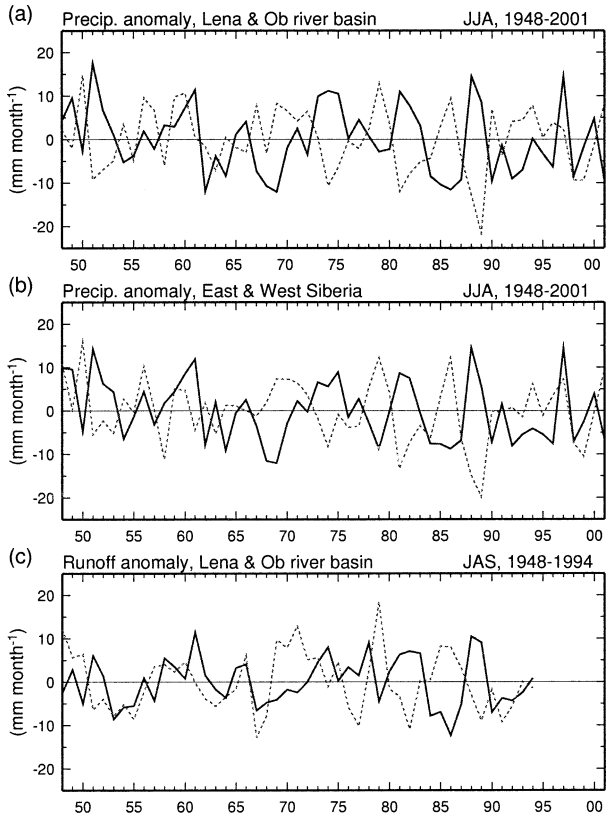

FIG. 9. (a) The time series of area-averaged precipitation anomalies for JJA 1948–2001. Thick solid (thin dashed) line indicates the series for the Lena (Ob) basin. (b) The same as (a) except for the east (50°–70°N, 95°–135°E) and west (50°–70°N, 55°–95°E) Siberian domain. (c) The same as (a) except for the river runoff for JAS 1948–94. The river gauge station for the Lena is located at Kusur.

Pacific that corresponds well with the pattern in Fig. 7, in that it shows large-amplitude anomalies appearing over the east Pacific, North America, and Atlantic regions. This REOF 1 mode explains 15.7% of the total variance. Here, note that this Eurasian wave pattern was also determined as a second EOF mode derived before the REOF analysis.

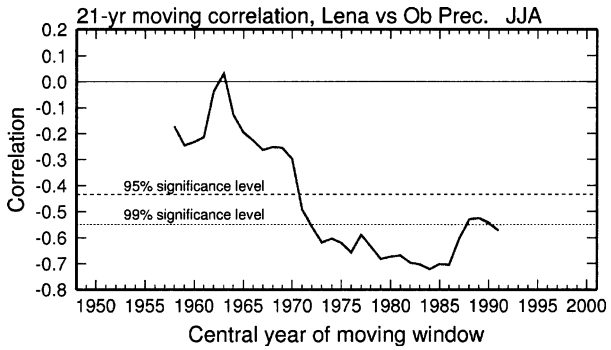

FIG. 10. A 21-yr moving cross correlation between the Lena and Ob precipitation index for JJA during 1948–2001. The dashed line indicates the 95% significance level.

The time series of the REOF 1 score (denoted as RPC 1) is shown in Fig. 8b, combined with the precipitation index for each basin. Although biennial-like signals are dominant during the early 1980s and early 1990s in REOF 1, it also appears to contain longer-timescale (more than 6-yr period) components. In fact, the RPC 1 time series is most highly correlated with the precipitation index for the Lena and Ob of all the RPC scores. The significant positive correlation between RPC 1 and the Lena index (0.52) is most important, as is the significant negative correlation between RPC 1 and the Ob index (-0.52). From the time series plots (Fig. 8b), the nearly in-phase relationship between RPC 1 and the Lena index, and the out-of-phase relationship for the Ob, are evident.

c. Robustness of the seesawlike dry and wet regimes

The results presented in this paper suggest the existence of an east–west seesawlike alternation of summer dry and wet regimes on the interannual timescale in the Siberian domain. As aforementioned, it appears to have a 6–8-yr cycle. However, our results have not completely determined the 6–8-yr quasi-periodical signals in precipitation. Fundamental questions still remain. Is the summer precipitation seesaw on this longer interannual timescale a robust signal? Our main analyses in the previous sections are limited for the period after 1979. Here, we further examined long-term changes of basin-scale precipitation and runoff for this issue. Therefore, the monthly precipitation record spanning the 54-yr period (see section 2) was used for the additional analysis that follows.

Figure 9 displays simple comparisons of summer precipitation (JJA 1948–2001) and runoff (JAS 1948–94) index between the Lena and Ob area. In the basin-averaged precipitation index (Fig. 9a), an out-of-phase relationship with a nearly 6–8-yr cycle and associated replacement of wet and dry regimes are evident from the middle 1970s through 1980s. In contrast, this characteristic is not found in the period from the middle 1950s through 1960s. Similar variation features are identified also in the area-averaged precipitation series for east and west Siberia (Fig. 9b). The Lena and Ob runoff time series (Fig. 9c) appear to well reflect the precipitation tendencies on interannual and decadal timescales. While these two tend to be out of phase with each other, particularly for the 15-yr period from the middle 1970s, they appear to keep nearly in-phase variations from the middle 1950s through late 1960s. Obviously, the 6–8-yr cycle signal after 1979 shown in the previous section constitute a part of about 2.5 cycles of this that last from the 1970s through the 1980s in Fig. 9. A changing relationship between the Lena and Ob precipitation index can be statistically identified by the 21-yr moving cross correlation (Fig. 10). The negative correlation well exceeds the 95% significance level after the early 1970s, which supports the emergence of the

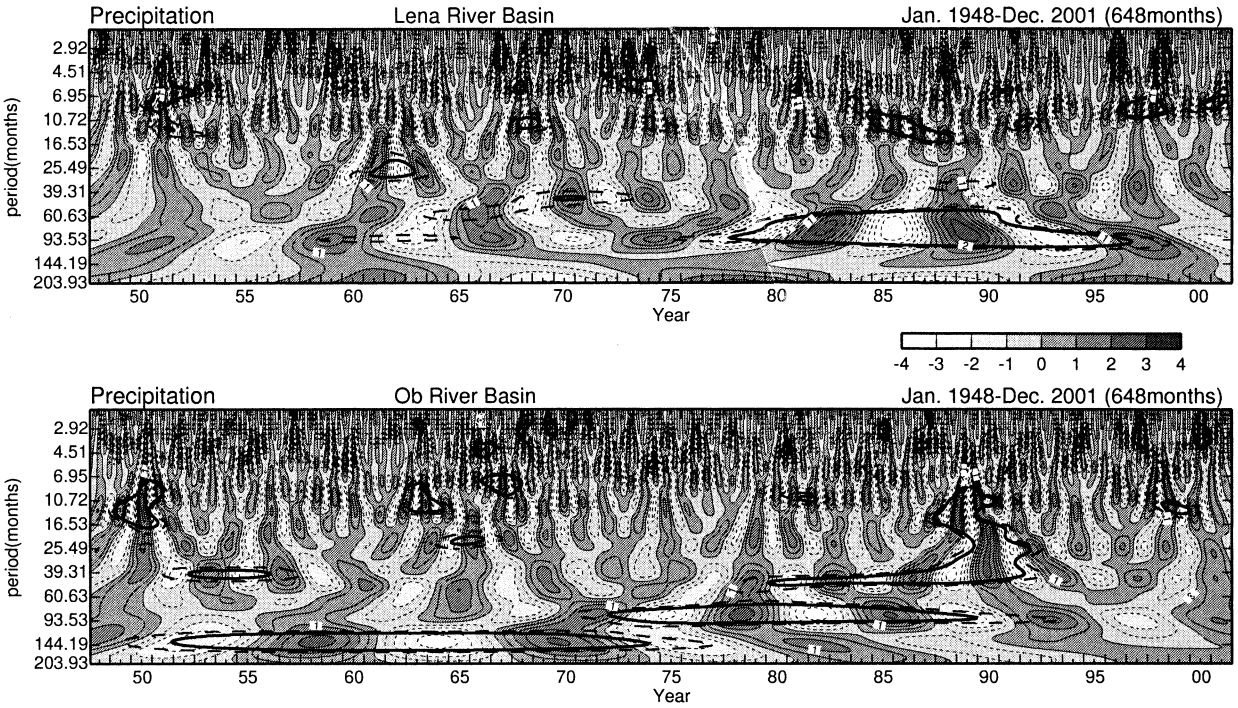

FIG. 11. Real part of Morlet wavelet transform of monthly precipitation index for (a) the Lena River basin and (b) the Ob River basin during 54-yr period from 1948–2001 (648 months). The real part of wavelet coefficient is normalized by the std dev. The solid and dashed contours indicate the 95% and 90% significance levels, respectively.

dominant out-of-phase relationship between them during the last 25–30 yr. In contrast, these two precipitation time series are actually incoherent with respect to each other before this epoch. Both the in-phase and out-of-phase relationship is not robust from the 1950s through the 1960s.

To clarify the quasi periodicity of 6–8 yr in the precipitation variation for these two basins, wavelet analysis is applied based on the method developed by Torrence and Compo (1998). Figure 11 displays the real part of the Morlet wavelet coefficients for the entire 54-yr record (648 months). Prior to this analysis, monthly climatological annual cycle and linear trend are subtracted from each precipitation index. The upper panel (Fig. 11a) clearly shows the strong signal in the 6–8-yr range of the Lena precipitation index, and this signal is 90% statistically significant from 1975 through 1998. A corresponding signal is also seen in the Ob index (Fig. 11b), which has a 90% significant area spanning 1971 through 1993. These two signals apparently exhibit an out-of-phase pattern with each other after 1972. Furthermore, we examined a wavelet spectrum of each seasonal mean precipitation time series over the 54-yr period (not shown). The seasons were simply defined as JJA, SON (September–November), DJF (December–February), and MAM (March–May). As a result, the 6–8-yr signals were evident only in the wavelet spectrum for the summer mean (JJA) precipitation indices. Statistical properties in the analysis results verify the robustness of the out-of-phase summer precipitation variation between the Lena and Ob since the early 1970s. Here, we can also notice that the Ob spectrum (Fig. 11b) includes a decadal signal during 1950–76 and a 4–5-yr signal during 1978–92; however, it is beyond the scope of this paper to discuss these variabilities.

Finally in this section, the summer atmospheric patterns are examined to ensure the robustness of the Eurasian wave structure during the period when the pronounced precipitation seesaw is observed. The last 30-yr (1972–2001) record of the NCEP–NCAR reanalysis and PREC/L-based precipitation index are used. Note that each precipitation index was detrended. The resulting regression maps of 500-hPa geopotential height anomalies against the Lena and Ob precipitation index are given in Fig. 12. The basic features, especially the east–west dipole structures are strongly similar to those in Fig. 7. This fact gives us reasonable confidence in the presence of this type of atmospheric pattern associated with the northern Eurasian precipitation seesaw.

5. Discussion

It is interesting to note that similar timescale fluctuations in Eurasian hydrometeorological components have been detected by several past studies. Semiletov et al. (2000) and Savelieva and Semiletov (2001) confirmed the existence of 6–8-yr-period variations of annual runoff, precipitation, and temperature in Siberian

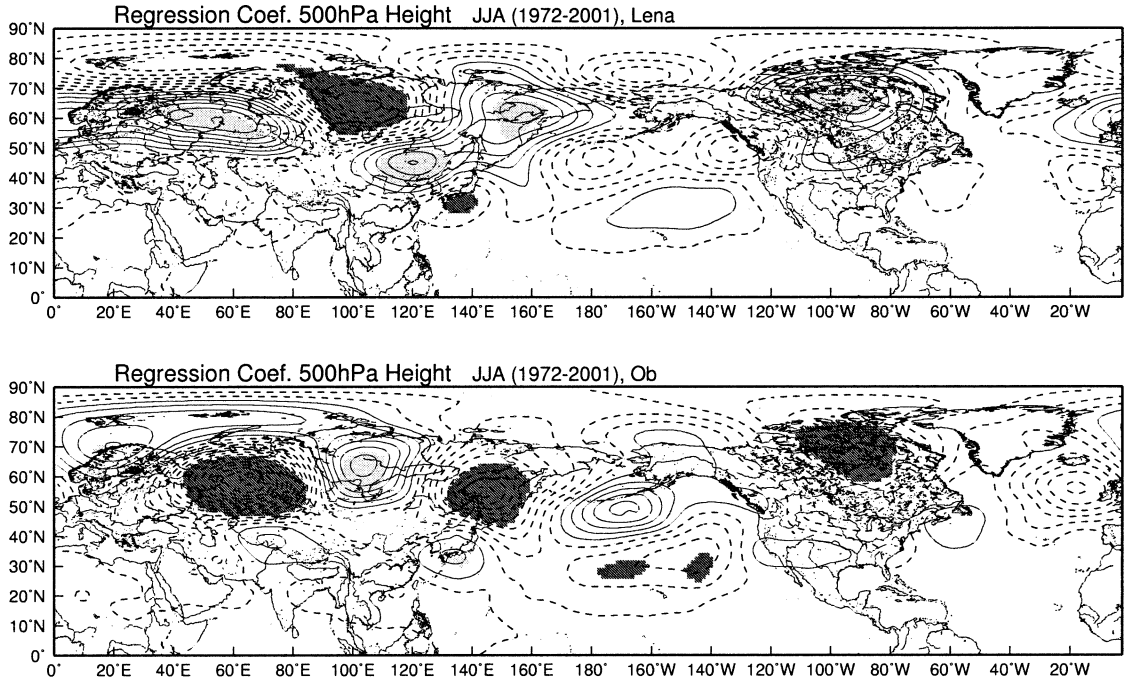

FIG. 12. (a) The regression map of the Northern Hemisphere 500-hPa geopotential height field (m) based upon the JJA precipitation index for the Lena River basin during 30-yr period from 1972 to 2001. Contour interval is 2 m. Negative values are drawn with dashed contours. Zero contours are omitted. The 95% statistically significant areas are shaded. (b) As in (a) except for the Ob index.

river basins. One can also find a similar signal of Ob runoff after 1970 in the results of Johnson et al. (1999), which is based on the 3-yr smoothed monthly record (in their Fig. 5). As shown in our Figs. 9, 10, and 11 and some previous results, the 6–8-yr variations with out-of-phase signatures in summer precipitation and runoff are likely to have been initiated in the early 1970s. Savelieva et al. (2000) pointed out that the decadal climate regime shift over northern Eurasia and the North Pacific in the 1970s had significant influences on the hydrological variations for Siberia. This wintertime climate shift with a pan-Pacific scale has been reported by many previous studies as noted by Minobe (2000). Besides, the impact of this on the summer monsoon–ENSO relationship is proposed by Chang et al. (2001) and Kinter et al. (2002). However, the direct link between this regime shift and the appearance of the 6–8-yr signals (Fig. 9) is still unclear.

As described at the beginning of this paper, the factor to regulate the northern Eurasian dry and wet regimes is a primary concern. It is natural to ask what factors excite the Eurasian wave pattern that alternates the summer precipitation and associated hydrological cycles? A relation with the large-scale mode of atmospheric variations is an unresolved issue. Park and Schubert (1997) discussed the causes for summer Eurasian stationary waves in terms of orographic forcing and remote response to the monsoon. They also noted the possible roles of atmospheric conditions in the preceding season on generating the midlatitude wave anomalies. Yasunari et al. (1991) give an insight into the effect of the atmosphere–land interactions and land memory in the preceding seasons on the summertime mid- and high-latitude circulations over Eurasia. However, the generation of the 6–8-yr cycles observed in northern Eurasia itself could not be explained by only these factors. We need to examine the land-memory effect during the spring to early-summer season on the summer atmospheric conditions and hydrological cycle in current GCM results. For example, outputs reproduced by AMIP-II models can be useful to diagnose these factors.

Now, another possibility may be a close association with the subdecadal atmospheric mode on a 6–7-yr timescale obtained by Venegas and Mysak (2000). They isolated this timescale mode by coupling sea ice anomalies in the North Atlantic–Arctic Ocean (Greenland and Irminger Seas) to hemispheric sea level pressure anomalies. In their Fig. 8, there is an evident recurrent cycle of sea level pressure anomalies that forms a hemispheric wavelike pattern. In addition, variation on a similar timescale has been noticed in global temperature (Mann and Park 1994), Arctic sea ice anomalies (Arfeuille et al. 2000), and the North Atlantic Oscillation (e.g., Hurrell and van Loon 1997; Pozo-Vázquez et al. 2001; Costa and de Verdiere 2002). These earlier studies imply that the atmosphere–ocean coupling system in the North Atlantic domain may be an effective driving force for the hemispheric atmospheric mode at this timescale. The

best way to understand this is an examination from the viewpoint of the teleconnections between North Atlantic sea surface conditions (sea surface temperatures and sea ice extent) and subsequent Eurasian atmospheric conditions (e.g., Palmer and Sun 1985; Peng and Mysak 1993; Peng et al. 1995; Ting and Peng 1995). However, we would note that representative teleconnection indices have no significant correlation with Siberian hydrometeorological components for summer (e.g., Rogers et al. 2001; Serreze et al. 2002).

6. Conclusions

We investigated the characteristics of the summer water balance components over northern Eurasia, and revealed noticeable interannual signals. The variance in the summer (JJA) precipitation suggests that two centers of action for the hydrological cycle exist, one over eastern Siberia (including the Lena basin), and the other over western Siberia (including the Ob basin). The JJA precipitation correlates strongly with the mid- to late-summer runoff (JAS) in these two basins. In addition, their fluctuations in precipitation, moisture convergence, and runoff indicate the presence of 6–8-yr cycles. Dry and wet regimes are associated with these signals. Moreover, basin-scale precipitation variability indicates that the relatively wet and dry regimes in the Lena basin are essentially out of phase with those in the Ob basin.

We then examined the large-scale atmospheric moisture transport and circulation fields associated with basin-scale precipitation variability. The regression analysis results based on the precipitation index for these two basins (Lena and Ob Rivers) show contrasting features. When the Lena basin is wet, a cyclonic circulation (moisture flux) coupled with large positive precipitation anomalies entirely covers this basin, while at these times anticyclonic circulation collocated with negative precipitation anomalies prevail over the Ob basin. The east–west dipole structures of the circulation and precipitation anomalies are clearly evident. A seesawlike replacement of the dry and wet regimes associated with this dipole circulation structure occurs between eastern and western Siberia at this timescale.

The Eurasian wave patterns that emerge, correlated with the basin-scale precipitation variability, appear to be closely linked to the interannual leading mode of summer geopotential height anomalies over the Northern Hemisphere. The first REOF mode, which shows a hemispheric wavelike pattern, closely resembles the regression pattern of geopotential height anomalies in the precipitation index for each basin. This suggests that large-scale circulation anomalies with a hemispheric teleconnective pattern may be one of the causes for modulating the regional moisture transport and atmospheric water flow into these basins, and also the resulting precipitation and runoff. This is also strongly supported by the significant cross correlation between the precipitation index and the leading principal component time series.

Acknowledgments. We thank the three anonymous reviewers for their insightful comments on an earlier version of manuscript. We benefited from critical comments by John Walsh for improving the quality of this paper. Mark Serreze and David Bromwich kindly sent us their forthcoming paper. Part of the NCEP reanalysis-2 dataset was obtained from the NCEP. We would like to thank M. Kanamitsu (now at Scripps Institute of Oceanography), W. Ebisuzaki, and E. Yarosh who kindly helped us to access the data. The rest of this dataset was provided by the NCAR Data Support Section (DSS). The CMAP and PREC/L datasets were obtained from the NCEP–CPC (ftp://ftp.cpc.ncep.noaa.gov/precip). The Bodo-enhanced Russian river flow dataset is available at NCAR/DSS (ftp://dss.ucar.edu/ds553.2). The wavelet analysis tools developed by Torrence and Compo (1998) was taken from their Web site at the University of Colorado (http://monsoon.colorado.edu/research/wavelet). The Generic Mapping Tools (GMT) graphics package developed by Wessel and Smith (1995) was used in preparing all the figures.

APPENDIX

Climatology of Annual Water Balance for Three River Basins

Long-term annual means of water balance components estimated from the NCEP–DOE AMIP-II reanalysis and CMAP data are provided for the purpose of checking their accuracy. The main focus is whether the climatological precipitation minus evaporation ($P - E$) derived from reanalysis is close to runoff (R) or not in each river basin. In general, the long-term mean of $P - E$ and R should be equal in a theoretical sense. The values of these components are summarized in Table A1. The mean annual values are defined based on the hydrological year from October 1979 through September 1994 for the Lena and Ob (15 yr), and from October 1979 through September 1995 for the Yenisey (16 yr).

Comparing $P - E$ with R, these terms almost agree with each other for the Lena and Yenisey. On the other hand, the difference between these two components is much larger for the Ob (50 mm yr^{-1}). One of the pos-

TABLE A1. Climatological annual water budget for three river basins in Siberian domain (mm y^{-1}). $P - E$ is computed from R2, and P is derived from CMAP; E is estimated as the residual from these products.

	Annual P, $P - E$, E, and R			
	P	$P - E$	E	R
Lena	350	190	160	197
Yenisey	410	231	179	241
Ob	430	110	320	164

sible reasons for this large imbalance may be caused by underestimation of moisture convergence for the Ob.

In addition, the area-averaged precipitation for each basin computed from CMAP data is much smaller than that obtained from the gauge-corrected precipitation by Serreze et al. (2002). The major factor for this is presumably caused by the snow undercatchments at rain gauges during the cold season.

REFERENCES

Adams, J. C., and P. N. Swarztrauber, 1999: SPHEREPACK 3.0: A model development facility. *Mon. Wea. Rev.*, **127,** 1872–1878.

Arfeuille, G., L. A. Mysak, and L. B. Tremblay, 2000: Simulation of the interannual variability of the wind driven Arctic sea ice cover during 1958–1998. *Climate Dyn.,* **16,** 107–121.

Bjornsson, H., L. A. Mysak, and R. D. Brown, 1995: On the interannual variability of precipitation and runoff in the Mackenzie drainage basin. *Climate Dyn.,* **12,** 67–76.

Bowling, L. C., D. P. Lettenmaier, and B. V. Matheussen, 2000: Hydroclimatology of the Arctic drainage basin. *The Freshwater Budget of the Arctic Ocean,* E. L. Lewis, Ed., Kluwer Academic, 57–90.

Carmack, E. C., 2000: The Arctic Ocean's freshwater budget: Sources, storage and export. *The Freshwater Budget of the Arctic Ocean,* E. L. Lewis, Ed., Kluwer Academic, 91–126.

Chang, C.-P., P. Harr, and J. Ju, 2001: Possible roles of Atlantic circulations on the weakening Indian monsoon rainfall–ENSO relationship. *J. Climate,* **14,** 1203–1215.

Chen, M., P. Xie, J. E. Janowiak, and P. A. Arkin, 2002: Global land precipitation: A 50-yr monthly analysis based on gauge observations. *J. Hydrometeor.*, **3,** 249–266.

Chen, S. J., Y.-H. Kuo, P.-Z. Zhang, and Q.-F. Bai, 1991: Synoptic climatology of cyclogenesis over east Asia, 1958–1987. *Mon. Wea. Rev.,* **119,** 1407–1418.

Costa, E. D., and A. C. de Verdiere, 2002: The 7.7-year North Atlantic Oscillation. *Quart. J. Roy. Meteor. Soc.*, **128,** 797–817.

Cullather, R. I., D. H. Bromwich, and M. C. Serreze, 2000: The atmospheric hydrologic cycle over the Arctic basin from reanalyses. Part I: Comparison with observations and previous studies. *J. Climate*, **13,** 923–937.

Hurrell, J., and H. van Loon, 1997: Decadal variations in climate associated with the North Atlantic Oscillation. *Climatic Change*, **36,** 301–326.

Johnson, M., A. Proshutinsky, and I. Polyakov, 1999: Atmospheric patterns forcing two regimes of Arctic circulation: A return to anticyclonic conditions? *Geophys. Res. Lett.*, **26,** 1621–1624.

Kalnay, E., and Coauthors, 1996: The NCEP/NCAR 40-Year Reanalysis Project. *Bull. Amer. Meteor. Soc.*, **77,** 437–471.

Kanamitsu, M., W. Ebisuzaki, J. Woollen, S.-K. Yang, J. J. Hnilo, M. Fiorino, and G. L. Potter, 2002: NCEP–DOE AMIP-II Reanalysis (R2). *Bull. Amer. Meteor. Soc.*, **83,** 1631–1643.

Kinter, J., K. Miyakoda, and S. Yang, 2002: Recent changes in the connection from the Asian monsoon and ENSO. *J. Climate*, **15,** 1203–1215.

Kistler, R., and Coauthors, 2001: The NCEP/NCAR 50-year reanalysis: Monthly means CD-ROM and documentation. *Bull. Amer. Meteor. Soc.*, **82,** 247–268.

Kripalani, R. H., and A. Kulkarni, 1999: Relationship between the Indian monsoon rainfall and the tropospheric temperature over the Eurasian continent. *Climate Dyn.*, **15,** 475–489.

Manak, D. K., and L. A. Mysak, 1989: On the relationship between Arctic sea-ice anomalies and fluctuations in northern Canadian air temperature. *Atmos.–Ocean*, **27,** 682–691.

Mann, M. E., and J. Park, 1994: Global-scale modes of surface temperature variability on interannual to century timescales. *J. Geophys. Res.,* **99D,** 25 819–25 833.

Maurer, E. P., G. M. O'Donnel, D. P. Lettenmaier, and J. O. Roads, 2001: Evaluation of the land surface water budget in NCEP/NCAR and NCEP/DOE reanalysis using an off-line hydrologic model. *J. Geophys. Res.,* **106** (D), 17 841–17 862.

Minobe, S., 2000: Spatio-temporal structure of the pentadecadal variability over the North Pacific. *Progress in Oceanography*, Vol. 47, Pergamon, 381–408.

Mysak, L. A., D. K. Manak, and R. F. Marsden, 1990: Sea-ice anomalies observed in the Greenland and Labrador Seas during 1901–1984 and their relation to an interdecadal Arctic climate cycle. *Climate Dyn.,* **5,** 111–133.

Oki, T., K. Musiake, H. Matsuyama, and K. Masuda, 1995: Global atmospheric water balance and runoff from large river basins. *Hydrol. Processes,* **9,** 655–678.

——, T. Nishimura, and P. Dirmeyer, 1999: Assessment of annual runoff from land surface models using total runoff integrating pathways (TRIP). *J. Meteor. Soc. Japan,* **77,** 235–255.

Palmer, T. N., and Z. Sun, 1985: A modeling and observational study of the relationship between sea surface temperature in the northwest Atlantic and the atmospheric general circulation. *Quart. J. Roy. Meteor. Soc.*, **111,** 947–975.

Park, C.-K., and S. D. Schubert, 1997: On the nature of the 1994 East Asian summer drought. *J. Climate,* **10,** 1056–1070.

Peixoto, J. P., and A. H. Oort, 1992: *Physics of Climate.* Amer. Inst. Phys., 520 pp.

Peng, S., and L. A. Mysak, 1993: A teleconnection study of interannual sea surface temperature fluctuations in the northern North Atlantic and precipitation and runoff over western Siberia. *J. Climate*, **6,** 876–885.

——, ——, H. Ritchie, J. Derome, and B. Duas, 1995: The differences between early and midwinter atmospheric responses to sea surface temperature anomalies in the northwest Atlantic. *J. Climate*, **8,** 137–157.

Pozo-Vázquez, D., M. J. Esteban-Parra, F. S. Rodrigo, and Y. Castro-Diez, 2001: A study of NAO variability and its possible nonlinear influences on European surface temperature. *Climate Dyn.,* **17,** 701–715.

Rogers, A. N., D. H. Bromwich, E. N. Sinclair, and R. I. Cullather, 2001: The atmospheric hydrologic cycle over the Arctic basin from reanalyses. Part II: Interannual variability. *J. Climate,* **14,** 2414–2429.

Savelieva, N. I., and I. P. Semiletov, 2001: Siberian rivers input on the Arctic shelf in the 20th century and their feedback with climate. *Extended Abstracts, Second Wadati Conf. on Global Change and the Polar Climate,* Tsukuba, Japan, Geophysical Institute and International Arctic Research Center, 237–240.

——, ——, L. N. Vasilevskaya, and S. P. Pugach, 2000: A climate shift in seasonal values of meteorological and hydrological parameters for northeastern Asia. *Progress in Oceanography*, Vol. 47, Pergamon, 279–297.

Semiletov, I. P., N. I. Savelieva, G. E. Weller, I. I. Pipko, S. P. Pugach, A. Y. Gukov, and L. N. Vasilevskaya, 2000: The dispersion of Siberian river flows into coastal waters: Meteorological, hydrological and hydrochemical aspects. *The Freshwater Budget of the Arctic Ocean,* E. L. Lewis, Ed., Kluwer Academic, 323–366.

Serreze, M. C., M. P. Clark, A. J. Etringer, and D. H. Bromwich, 2001a: Variability and trends in the hydro-climatology of the major Eurasian Arctic drainages. *Extended Abstracts, Second Wadati Conf. on Global Change and the Polar Climate,* Tsukuba, Japan, Geophysical Institute and International Arctic Research Center, 83–86.

——, A. H. Lynch, and M. P. Clark, 2001b: The Arctic frontal zone as seen in the NCEP–NCAR reanalysis. *J. Climate*, **14,** 1550–1567.

——, D. H. Bromwich, M. P. Clark, A. J. Etringer, T. Zhang, and R. Lammers, 2003: The large-scale hydro-climatology of the terrestrial Arctic drainage basin. *J. Geophys. Res.*, in press.

Smirnov, V., and G. W. K. Moore, 1999: Spatial and temporal structure of atmospheric water vapor transport in the Mackenzie River basin. *J. Climate,* **12,** 681–696.

——, and ——, 2001: Short-term and seasonal variability of the

atmospheric water vapor transport through the Mackenzie River basin. *J. Hydrometeor.,* **2,** 441–452.

Ting, M., and S. Peng, 1995: Dynamics of the early and middle winter atmospheric responses to the northwest Atlantic SST anomalies. *J. Climate,* **8,** 2239–2254.

Torrence, C., and G. P. Compo, 1998: A practical guide to wavelet analysis. *Bull. Amer. Meteor. Soc.,* **79,** 61–78.

Trenberth, K. E., 1991: Climate diagnostics from global analyses: Conservation of mass in ECMWF analyses. *J. Climate,* **4,** 707–722.

——, 1999: Atmospheric moisture recycling: Role of advection and local evaporation. *J. Climate,* **12,** 1368–1381.

Venegas, S. A., and L. A. Mysak, 2000: Is there a dominant timescale of natural climate variability in the Arctic? *J. Climate,* **13,** 3412–3434.

Walsh, J. E., 2000: Global atmospheric circulation patterns and relationships to Arctic freshwater fluxes. *The Freshwater Budget of the Arctic Ocean,* E. L. Lewis, Ed., Kluwer Academic, 21–43.

——, X. Zhou, D. Portis, and M. C. Serreze, 1994: Atmospheric contribution to hydrologic variations in the Arctic. *Atmos.–Ocean,* **32,** 733–755.

Wang, X. L., and H. Cho, 1997: Spatial–temporal structures of trend and oscillatory variabilities of precipitation over Northern Eurasia. *J. Climate,* **10,** 2285–2298.

Wessel, P., and W. H. F. Smith, 1995: New version of the Generic Mapping Tools released. *Eos, Trans. Amer. Geophys. Union,* **76,** 329.

Xie, P., and P. A. Arkin, 1996: Analysis of global monthly precipitation using gauge observations, satellite estimates, and numerical model predictions. *J. Climate,* **9,** 840–858.

——, and ——, 1997: Global precipitation: A 17-year monthly analysis based on gauge observations, satellite estimates, and numerical model outputs. *Bull. Amer. Meteor. Soc.,* **78,** 2539–2557.

Yasunari, T., A. Kitoh, and T. Tokioka, 1991: Local and remote responses to excessive snow mass over Eurasia appearing in the northern spring and summer climate. *J. Meteor. Soc. Japan,* **69,** 473–487.

Ye, H., 2001: Characteristics of winter precipitation variation over northern central Eurasia and their connections to sea surface temperatures over the Atlantic and Pacific Oceans. *J. Climate,* **14,** 3140–3155.